Cell PRESS
Structure
Article

Fine Details of IGF-1R Activation, Inhibition, and Asymmetry Determined by Associated Hydrogen /Deuterium-Exchange and Peptide Mass Mapping

Damian Houde[1,*] and Stephen J. Demarest[2,3,*]
[1]Department of Analytical Development
[2]Department of Protein Biochemistry
Biogen Idec, Cambridge, MA 02142, USA
[3]Present address: Eli Lilly, 10300 Campus Point Drive, Suite 200, San Diego, CA 92121, USA
*Correspondence: demarestsj@lilly.com (S.J.D.), damian.houde@biogenidec.com (D.H.)
DOI 10.1016/j.str.2011.03.014

SUMMARY

The structural features of the asymmetric activated states of the insulin receptor family are still poorly understood. We investigated hydrogen/deuterium (H/D)-exchange within the extracellular domain of the type-I insulin-like growth factor receptor (IGF-1R) in the absence and presence of IGF-1 (active state) and in the presence of antibody inhibitors (inactive state). Near complete coverage of the 210 kDa receptor sequence was obtained by mass mapping of proteolytically derived peptides at all H/D-exchange time points. The data provide details regarding solvent exposure and dynamics across the extracellular region as well as conformational changes induced by activation or inactivation. Multiple peptides, distant in structure, individually demonstrated two distinct H/D-exchange rates, suggesting that each of these peptides exists in two separate environments in IGF-1R. The dual-exchange behavior of these peptides was enhanced on ligand binding and eliminated on inhibitor binding, clearly associating these regions with active state asymmetry and enabling them to serve as reporters of receptor activity.

INTRODUCTION

The type-I insulin-like growth factor receptor (IGF-1R) is a member of the insulin-receptor family of receptor tyrosine kinases. It plays essential roles in fetal and adolescent growth and development and in metabolism as part of its ancestral relationship to the insulin receptor (IR) (Clemmons, 2007). Insulin is the primary ligand for IR, and IGF-1 and IGF-2 are the ligands for IGF-1R. The ligands are structurally related to one another as are IGF-1R and IR (De Meyts and Whittaker, 2002). The mature form of IGF-1R, on the cell surface, is a homodimer of two independently synthesized polypeptide chains that are each cleaved in their extracellular domains by furin to produce a heterotetramer consisting of two N-terminal α- and two C-terminal β-chains (Adams et al., 2000). Each half of the heterotetrameric receptor (α- and β-chains) contains six extracellular domains consisting (from N to C terminus) of a receptor L domain (L1), a cysteine-rich region (CRR), another receptor L domain (L2), and 3 Type-III fibronectin domains (FnIII-1, FnIII-2, and FnIII-3). The FnIII-2 domain structure is interrupted by a large (~120 residue) insert domain that contains the furin cleavage site. Disulfide bonds covalently connect the α- and β-chains as well as each subunit of the homodimer (interdimer).

Ligand binding induces conformational changes in the extracellular region of IGF-1R that results in the activation of the intracellular tyrosine kinase domains. IGF-1R activation leads to recruitment and activation of various adaptor proteins that in turn promote a range of cellular responses, most notably cell survival and cell-cycle progression. The mitogenic and cell-survival activities of the IGF-1 and IGF-2 ligands have been shown to enhance the formation of atherosclerotic plaques as well as promote tumor growth (Clemmons, 2007; Pollak, 2008). Based on a wealth of preclinical data, epidemiology, and in rare cases the identification of direct genetic aberrations linked to cancer, IGF-1R has emerged as a strongly pursued target in oncology (Pollak, 2008). Both small molecule and antibody approaches are being tested in mid- and late-stage clinical trials for various forms of cancer.

As homodimers, both IR and IGF-1R hypothetically contain two identical ligand binding sites. However, the IR/IGF-1R systems are classical models of negative cooperativity. Using Scatchard analyses, ^{125}I-labeled ligands are competed off their receptors by unlabeled ligands in a curvilinear fashion with apparent high affinity and low affinity events (Christoffersen et al., 1994; De Meyts et al., 1973; Gavin et al., 1973). Additionally, unlabeled ligands induce enhanced dissociation of pre-bound ^{125}I-ligands from both IR and IGF-1R. This negative cooperativity requires significant regions of the receptors to be present, including domains L1, CRR, L2, FnIII-1, and exon 10, which encodes residues 704–719 of the insert domain (ID) (Surinya et al., 2002). The data strongly suggest an asymmetric receptor conformation in the ligand-bound state leading to the high- and low-affinity binding modes (De Meyts and Whittaker, 2002). However, very little regarding the defined structural features of the receptor in its active and asymmetric conformation has been defined since these discoveries in the early 1970s.

Monoclonal antibodies raised against either IR or IGF-1R can be relatively inert or can lead to enhanced or reduced ligand

binding, which is directly related to receptor activation (Soos et al., 1992; Soos et al., 1986). Inhibitory antibodies, which are under consideration for cancer therapy, can inhibit ligand binding in numerous ways ranging from purely allosteric inhibition to purely competitive inhibition (Doern et al., 2009). Two inhibitory antibodies, BIIB4 and BIIB5, are examples of purely competitive and purely allosteric inhibitors, respectively (Doern et al., 2009). BIIB5 (known externally as BIIB022) is currently being evaluated for its efficacy against various solid tumors in human clinical trials (Rodon et al., 2008).

New advances in rapid analytical separation procedures and mass spectrometry instrumentation have recently enabled the study of various proteins and protein complexes by mass spectrometry-based hydrogen/deuterium (H/D) exchange (Wales and Engen, 2006). The goal of the study described here was to examine the precise molecular details of the activated and inhibited states of IGF-1R by monitoring H/D-exchange of the receptor followed by proteolytic mass mapping of peptidic regions. As far as we know, the study of IGF-1R along with its activating and inhibitory modulators represents the largest protein studied to date by H/D-exchange mass spectrometry. First, we analyzed the H/D-exchange properties of IGF-1R in the absence (apo-state) or presence of IGF-1 (i.e., bound state) to precisely identify conformational changes within the receptor associated with activation. We chose IGF-1 instead of IGF-2 because IGF-1 has a higher affinity for the receptor and high serum concentrations of IGF-1 are associated with an increased risk and severity of cancer (Clemmons, 2007; Pollak, 2008). Finally, we studied the H/D-exchange properties of IGF-1R in the presence of the antibody inhibitors BIIB4 and BIIB5 to help define conformational features of the inactive state of the receptor and to provide mechanistic details regarding antibody-mediated inhibition.

RESULTS

Generation of a Peptide Map for Enzymatically Deglycosylated hIGF-1R(1–903)

To simplify the peptide map generated by proteolysis and liquid chromatography/mass spectrometry (LC/MS), hIGF-1R(1-903) (a recombinant protein consisting of the entire extracellular region of the human receptor) was enzymatically deglycosylated by overnight treatment with PNGaseF. The PNGaseF-treated protein was re-purified using preparative size exclusion chromatography (SEC) (Figure 1A) and maintained its monodisperse homodimeric structure. SDS-PAGE analysis (Figure 1B) showed a reduction in the apparent molecular weight for the PNGaseF-treated material both in the α- and β-chains. Static light scattering indicated a total molecular size decrease of $\sim$35 kDa after enzymatic treatment (data not shown), which is consistent with the loss of N-linked glycans from hIGF-1R(1–903). The deglycosylated protein was shown to maintain identical binding to both IGF-1 and the antibody Fab domains of BIIB4 (competitive inhibitor) and BIIB5 (allosteric inhibitor) (Figures 1C and 1D). Differential scanning calorimetry (DSC) analyses indicated only a small perturbation in the thermal stability of the hIGF-1R(1–903) after deglycosylation (Figure 1E). These data all suggest that deglycosylation did not have a big impact on the folding/activity of the protein.

The characterized peptide map of hIGF-1R(1–903) had near complete (94%) coverage of the receptor extracellular domain. After low pH proteolysis followed by LC/MS, 207 peptides were unambiguously identified. IGF-1R contains 16 putative N-linked glycosylation sites. Most are predicted to be occupied based on an analysis of the glycosylation patterns of IR (Adams et al., 2000). Subsequent to enzymatic treatment, aglycosyl peptides were identified in the peptide map that encompassed 14 of 16 putative N-linked glycosylation sites (only asparagines 214 and 717 were not identified). The inability to identify peptides containing asparagines 214 and 717 does not provide information regarding the glycosylation state of these sites.

H/D-Exchange within hIGF-1R(1–903)

The phenomenon of H/D-exchange has been extensively reviewed (Englander and Kallenbach, 1983; Wales and Engen, 2006). Briefly, in proteins H/D-exchange occurs at labile hydrogen atom positions, whereby hydrogen atoms spontaneously change places with other hydrogen atoms in the surrounding solvent. Hydrogens at the backbone amide positions are of particular interest, because variations in their chemical and physical environment induced by protein structure affect the rates of exchange over several orders of magnitude (Smith et al., 1997). Therefore, information concerning the conformation of a protein (or of differences between proteins) can be extracted by monitoring the exchange reaction. It should be noted, when comparing protein regions with very high or very little structural density (i.e., where exchange occurs extremely slow or fast), differences in H/D-exchange will likely not be detected and it is generally presumed that these regions are not involved in any structural perturbation.

Near complete peptide map coverage of hIGF-1R(1–903) enabled detailed determination of the H/D-exchange dynamics of peptides from each domain of the protein (see Table S1 available online). H/D-exchange was determined by measuring the centroid of each peptide's mass envelope and comparing this value to that determined in the absence of deuterium. The normalized H/D-exchange behavior of all 207 identified peptides is graphed in Figure 2. Consistent with the stably folded nature of the receptor, all peptides on average only exchanged 22% of their amide protons with solvent after four hours of deuterium exposure under ambient conditions at neutral pH. By domain, the CRR region had the highest level of exchange (and the most rapid, Figure 2), consistent with its relatively absent hydrophobic core. Several peptides located in the CRR region reached a maximum level of exchange at 10 s, which did not change even after 4 hr of exchange (Figure 2; Table S1). In these areas, H/D-exchange may occur too quickly to capture any changes in dynamics. Conversely, the L1 and L2 domains displayed the highest levels of protection (L1 = 18%, CRR = 34%, L2 = 15%, FnIII-1 = 27%, FnIII-2 = 23%, ID = 30%, FnIII-3 = 22%). Interestingly, the ID region was significantly protected from solvent, suggesting that it may not be as unstructured as is commonly believed (Adams et al., 2000).

Ligand-Induced Changes in the H/D-Exchange Behavior of hIGF-1R(1–903)

The H/D-exchange behavior of hIGF-1R(1–903) was also monitored in the presence of saturating levels of IGF-1 under

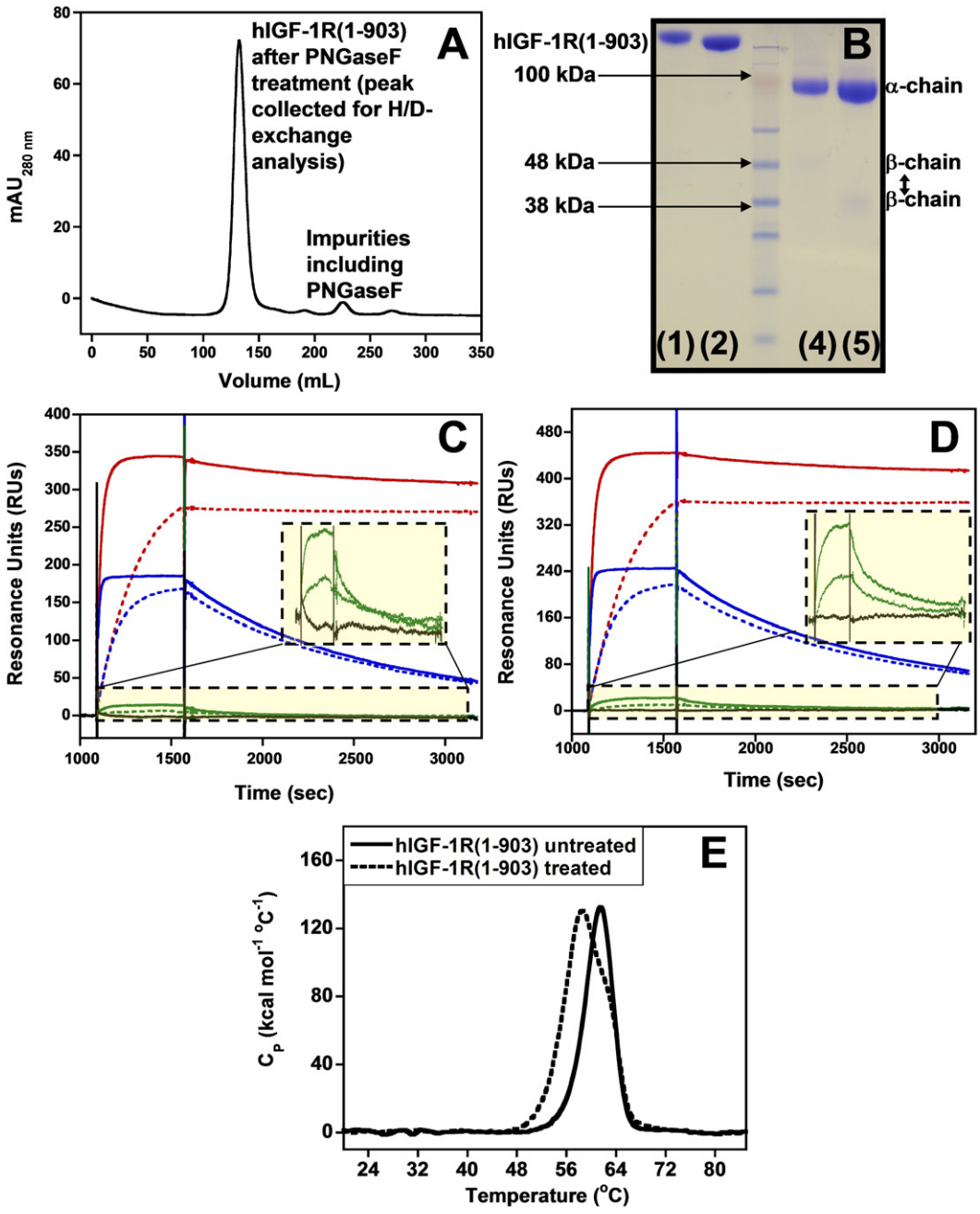

Figure 1. Purification and Characterization of Deglycosylated hIGF-1R(1–903)

(A) Preparative SEC profile of hIGF-1R(1–903) protein (elution peak at ~130 ml) subsequent to overnight treatment with PNGaseF.

(B) SDS-PAGE gel analysis of hIGF-1R(1–903) before and after treatment with PNGaseF. Lanes 1 and 2 are the protein before and after treatment, respectively, under nonreducing conditions, and lanes 4 and 5 are the protein before and after treatment, respectively, after heat treatment in 200 mM DTT (reducing conditions).

(C and D) Kinetic SPR binding curves obtained for the binding of IGF-1 at 5 nM (solid green line) and 50 nM (dashed green line), BIIB4 Fab at 3 nM (solid red line) and 30 nM (dashed red line), and BIIB5 Fab at 3 nM (solid blue line) and 30 nM (dashed blue line) to hIGF-1R(1–903) before (C) and subsequent to (D) treatment with PNGaseF. The insets have a modified y axis to more clearly show IGF-1 binding.

(E) DSC unfolding curves of hIGF-1R(1–903) before and after treatment with PNGaseF. See also Table S1.

conditions where ~99% of the receptor is expected to be occupied at all times (Doern et al., 2009). Representative plots of hIGF-1R(1–903) peptides displaying similar and differing H/D-exchange behavior in the absence and presence of IGF-1 are shown in Figures 3A and 3B, respectively. Differences in the H/D-exchange behavior of hIGF-1R peptides induced by IGF-1 binding are listed in Table 1 and mapped to the surface of the crystal structure of the homologous insulin receptor in Figure 4A

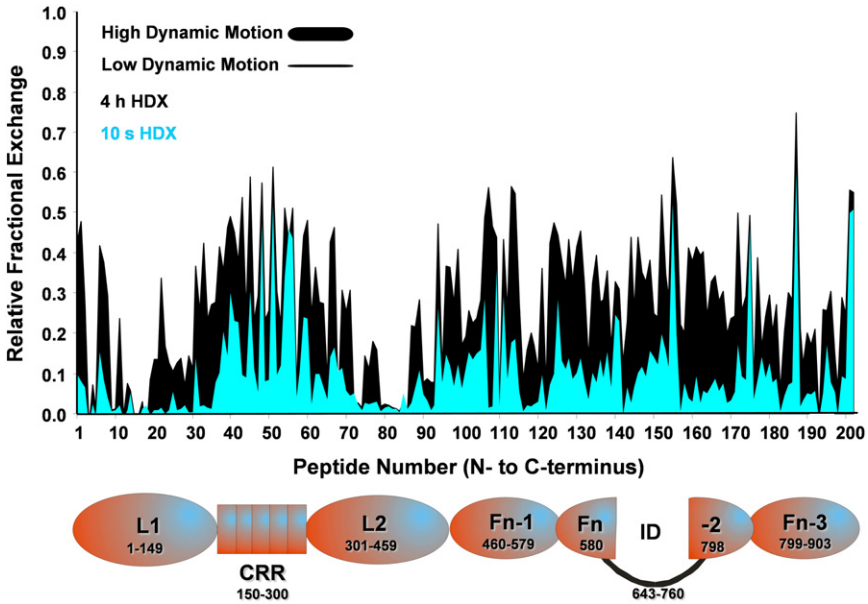

Figure 2. H/D Incorporation across hIGF-1R(1–903)

H/D incorporation across hIGF-1R(1–903) at 10 s (cyan) and 240 min (black), determined by pH quenching followed by low temperature and low pH proteolysis and LC-MS analysis. The plot shows the relative H/D incorporation of every detectable hIGF-1R(1–903) peptide from the N terminus (left) to C terminus (right). The H/D-exchange data was normalized to a fractional exchange value by dividing the observed level of H/D-exchange within each peptide by the total number of exchangeable residues within that peptide. For orientation of all hIGF-1R peptides along the x axis, an arbitrary peptide number was assigned to each peptide by summing the residue numbers at the start and end of each peptide and dividing the value by 2. The lowest value was assigned 1, the next lowest value was assigned 2, and so forth. In this format, the H/D-exchange of every identified peptide could be shown in a single plot. The H/D-exchange of all other time points (1, 10, and 60 min) are represented within the region between the cyan and black traces as the thickness of the black line. The line thickness also serves as an indicator for the level of backbone dynamics, where continual increases in H/D-exchange over the time course will produce a thick line and low or no H/D-exchange over the time course will produce a thin line. The schematic diagram below the graph roughly tracks the domain of IGF-1R from which each peptide was derived. The domain boundaries were defined previously (Adams et al., 2000).

(McKern et al., 2006). Significant changes in H/D-exchange were not observed in L1, even though this region is known to make many key contacts with ligand (Whittaker et al., 2001). One explanation is that many of the amide protons from residues within the L1 region known to be crucial for IGF-1 binding are highly protected from solvent in the apo-state and therefore do not become more protected in the IGF-1-bound state. For example, hIGF-1R peptides consisting of residues 28–33 and 75–79, which form a large portion of the ligand-binding surface within the L1 domain (Whittaker et al., 2001) show virtually no H/D-exchange in the apo-state (Table S1) and thus are not protected further in the IGF-1-bound state. The analysis does not provide information regarding changes in solvent exposure or hydrogen bonding within side chains. Amide protection was observed in a peptide (localized to residues 239–246 of the CRR region) within the ligand binding pocket known to be important for IGF-1 binding (Whittaker et al., 2001).

The most prominent areas of hIGF-1R(1–903) demonstrating changes in H/D-exchange behavior on ligand binding occur within the L2 and FnIII-1 domains near the homodimeric interface and within the ID (McKern et al., 2006). IGF-1-induced changes in the H/D-exchange behavior of residues near the homodimeric interface likely reflect a conformational change within the receptor that results in concerted changes in both subunits of the homodimer. Alanine-scanning mutagenesis of residues 692–701 within the ID has demonstrated that this region plays an important role in IGF-1 binding (Whittaker et al., 2001). Consistent with these results, we found that this region becomes significantly protected from H/D-exchange in the presence of ligand (Table 1).

Changes in hIGF-1R(1–903) H/D-Exchange on Binding of Antibody Inhibitors

BIIB4 and BIIB5 are competitive and allosteric inhibitors of IGF-1R, respectively (Doern et al., 2009). The BIIB4 epitope was localized to the CRR region and overlaps significantly with residues known to play a role in ligand binding, whereas the BIIB5 epitope was localized to the FnIII-1 domain distal to the ligand binding pocket (Doern et al., 2009). Binding of the BIIB4 and BIIB5 Fabs both induced significant changes in the H/D-exchange behavior of hIGF-1R(1–903) well beyond their known epitopes. Peptides whose H/D-exchange rates were modified by BIIB4 or BIIB5 binding are listed in Table 1 and mapped to the crystal structure of the insulin receptor (McKern et al., 2006) in Figures 4B and 4C, respectively.

Consistent with it being a competitive inhibitor of ligand binding, BIIB4 led to significant protection in both the L1 and CRR region in areas known to be important for ligand binding (Table 1 and Figure 4B) (Whittaker et al., 2001). Surprisingly, many of the BIIB4-induced changes in H/D exchange coincide with changes induced by IGF-1. However, two peptides were found (428–448 and 628–648) where IGF-1 led to reduced H/D-exchange whereas BIIB4 accelerated H/D-exchange.

BIIB5 is an allosteric inhibitor that binds the FnIII-1 domain of IGF-1R (Doern et al., 2009). The H/D-exchange data agrees well with what is known regarding BIIB5's epitope. On binding BIIB5, a hIGF-1R peptide encompassing residues 465–486, which contains many of the residues known to impact BIIB5 binding to the receptor, becomes protected from H/D-exchange (Table 1 and Figure 4C). BIIB5 also induced changes in H/D-exchange behavior within the IGF-1R homodimeric interface region and within the ID domain. An area within the ligand-binding pocket on the L1 domain becomes more labile to exchange (residues 81–86) on BIIB5 binding (Table 1).

Asymmetric H/D-Exchange Patterns within IGF-1R that Can Be Altered by Agonist/Antagonist Binding

Two hIGF-1R peptides consistently demonstrated peculiar H/D-exchange profiles that could not be explained by EX1 or

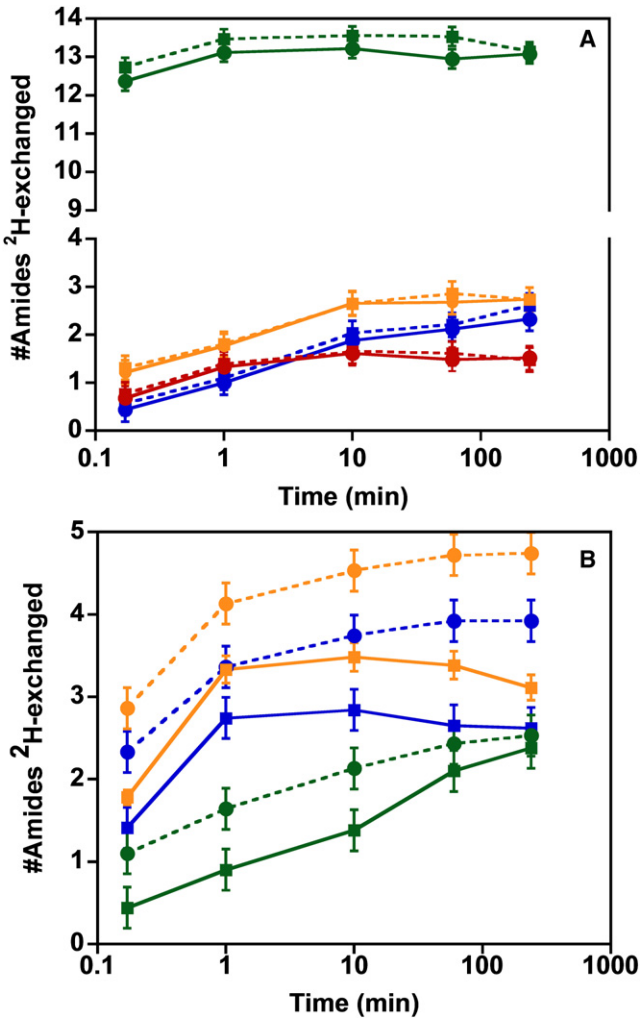

Figure 3. Time Course of H/D-Exchange within Peptides Derived from hIGF-1R(1–903)

H/D exchange was measured in the absence (■, dotted line) and presence (●, solid line) of a saturating level of hIGF-1. The plots show representative peptides with no difference (A) or a significant difference (B) in exchange behavior in the presence or absence of IGF-1 based on the centroid of their mass envelopes. (A) Blue = residues 1–8; green = 204–228; orange = 333–339; red = 735–740. (B) Blue = residues 428–448; green = 544–551; orange = 628–649. Residues 204–228 within the CRR region demonstrate significant exchange (>50% amide exchange) in both the apo- and IGF-1-bound states, suggesting this region is significantly exposed to solvent. Error bars indicate the standard error determined over an average of three experiments.

simple EX2 H/D-exchange mechanisms (428–448 and 628–648) (Weis et al., 2006b). Shown in Figure 5A is a typical EX2-type shift in the mass envelope of a peptide (residues 466–489) over time on exposure to deuterium at neutral pH at ambient temperature (apo-IGF-1R state). Nearly all the hIGF-1R(1–903) peptides demonstrated this uniform EX2-type exchange behavior. However, the mass envelopes of peptides consisting of residues 428–448 (within the L2 domain near the interface with FnIII-1) and 628–648 (within FnIII-2 at the junction with the ID) split into two mass envelopes, one that is largely protected from H/D-exchange and one that exchanges more rapidly (Figures 5B and 5C). This phenomenon could be distinguished from EX1-type exchange because both envelopes demonstrated a shift in the centroid of their mass envelopes relative to the unexchanged peptide per unit exchange time, which is consistent with EX2 exchange. In an EX1 scenario, the unexchanged mass envelope would be expected to decrease in population over time, whereas the fully exchanged mass envelope would be expected to increase proportionally, which does not correlate with the phenomenon observed here. Continuous injections of a protein sample have also been shown to cause false EX1-like exchange profiles, resulting from peptide carryover (Fang et al., 2011). However, this occurrence was ruled out: each protein sample was followed by a rigorous washing and two buffer blank injections, both of which showed no evidence of peptide carryover. Instead, these peptides seem to exist in two distinctly different chemical environments, one protected from exchange and one that exchanges more readily (Figures 5B and 5C). Some peptides that overlapped in primary sequences did not demonstrate these two separately exchanging populations. Therefore, the regions involved in this asymmetric exchange could be further localized to residues 428–437 and 641–648 of IGF-1R.

Next, the effect of adding an agonist (IGF-1) or antagonists (inhibitory antibodies) on the populations of the two apparently distinct chemical states was assessed. Interestingly, in the presence of IGF-1, the protected state in both the 428–448 and 628–648 peptides increased significantly (Figures 6A and 6B). The antibody antagonists, BIIB4 and BIIB5, both had large effects on the asymmetric H/D-exchange behavior discovered within hIGF-1R(1–903). Opposite to what was observed in the presence of IGF-1, both antibody Fabs eliminated the protected state within peptide 428–448 (Figure 6B). Within peptide 628–648, BIIB4, the competitive inhibitor, eliminated the protected state, whereas BIIB5 led to a slightly higher population of the protected state similar to what was observed with IGF-1 (Figure 6C).

DISCUSSION

The H/D-exchange data agree well with what is known regarding the structural features of IGF-1R (Garrett et al., 1998; McKern et al., 2006) and provide additional information regarding dynamics and accessibility across the receptor. Unsurprisingly, the CRR region, which lacks a hydrophobic core, exchanges the most extensively and most rapidly compared with other domains of IGF-1R (Figure 2). However, the relatively slow H/D-exchange behavior within the ID (similar to the H/D-exchange observed for the FnIII domains as a whole) was unanticipated (Figure 2). The ID is known to be mobile and make long-range contacts with the N-terminal L1 domain of the receptor in the ligand-bound state (Ward et al., 2008). The ID is often depicted as a relatively unstructured or loosely organized polypeptide whose interactions with other regions of the receptor are modified by IGF binding. The data here suggest that the ID domain, although mobile, is organized in some fashion that precludes rapid and extensive H/D-exchange.

The binding of IGF-1 led to both expected and unexpected changes in H/D-exchange patterns within the receptor. Correlating well with what is known regarding the ligand-binding pocket (Whittaker et al., 2001), residues within the CRR

Table 1. Changes in hIGF-1R(1–903) H/D-Exchange in the Absence or Presence of IGF-1 or Inhibitory Antibodies

IGF-1R Peptide	IR Structure Residue No. (2dtg)	H/D-Level Apo – Bound (1 min)	H/D-Level Apo – Bound (10 min)	H/D-Level Apo – Bound (60 min)	H/D-Level Apo – Bound (240 min)
IGF-1					
138–156	144–163	0.4	0.0	0.4	0.9
239–261[a]	246–253	0.7	0.3	0.6	0.0
298–315	308–325	0.5	0.3	0.5	0.0
327–356	337–366	0.6	0.6	0.7	0.1
428–448[a,b]	438–458	0.6	0.9	1.3	1.3
480–489	490–499	0.7	0.5	0.6	0.2
544–551	559–566	0.7	0.8	0.3	0.2
572–579	586–593	−0.2	−0.7	−0.3	−0.1
628–648[a,b]	642–662	0.8	1.1	1.3	1.6
696–701	xxxxxx	0.7	0.2	0.1	0.0
BIIB4					
33–47	37–53	0.5	0.5	0.7	0.7
87–109[a]	93–115	1.8	1.4	0.8	2.1
172–196	179–203	0.7	0.3	0.4	−0.3
229–248	236–255	0.3	0.8	0.7	1.0
284–312	295–322	−0.1	0.1	1.3	0.7
323–341	333–351	0.2	0.4	0.3	0.3
331–349	341–359	0.1	−1.0	−1.3	−1.2
428–448[b]	438–458	-2.2	-3.3	-2.8	-3.1
451–474	461–485	2.0	1.8	1.2	1.0
463–475	474–486	0.1	0.4	0.4	0.4
524–550	534–565	0.1	0.6	0.5	0.7
555–569	569–583	1.0	0.0	0.3	0.4
556–571	570–585	−0.1	0.2	0.3	0.6
628–648[b]	642–662	−0.8	−1.4	−1.9	−1.1
783–812	793–822	0.6	0.9	−0.1	−0.3
BIIB5					
81–86	87–92	0.0	−0.9	−0.7	−0.7
428–448[b]	438–458	—	−2.3	−1.7	−1.9
465–486	476–497	0.4	0.4	0.5	0.5
558–571	572–585	−0.8	−0.8	−1.2	−1.2
628–648[b]	642–662	1.2	0.7	1.0	1.2
719–732	xxxxxx	1.3	0.9	0.7	0.9
819–832	829–842	0.0	0.1	0.2	0.2

IR, insulin receptor.
[a] Changes in H/D-exchange on IGF-1 or BIIB4 binding can be localized to smaller regions based on data from overlapping peptides (i.e., 239–246, 428–437, and 641–648, respectively, for IGF-1 and 87–92 for BIIB4).
[b] Peptide demonstrates two separate H/D-exchange patterns. Changes in H/D incorporation are based on the average mass of the two mass envelopes.

(239–244), L2 (323–349, 451–474), and ID (696–701) that either face the ligand-binding pocket or have been shown to be important for ligand binding undergo protection from H/D-exchange in the presence of IGF-1. Interestingly, IGF-1R residues 696–701 are adjacent to residues 688-695 (residues 701–708 of IR), which have been shown recently to be part of a helical segment of the ID within IR called the αCT that packs against the L1 domain and completes the ligand binding site of the receptor (Smith et al., 2010). Based on alanine-scanning mutagenesis of IGF-1R, Whittaker et al. (2001) have demonstrated the critical nature of IGF-1R residue F701 and to a lesser extent residues 696, 697, 698, and 700 for maintaining a strong interaction with IGF-1. Thus, the interaction of residues 688–695 of the αCT peptide of IGF-1R (701–708 of IR) appear to pin the helical αCT segment against the L1 domain (Smith et al., 2010), whereas residues 696–701 (709–714 of IR) likely make strong direct contacts with ligand based on the H/D-exchange protection afforded by the addition of ligand. IGF-1 binding also led to changes in

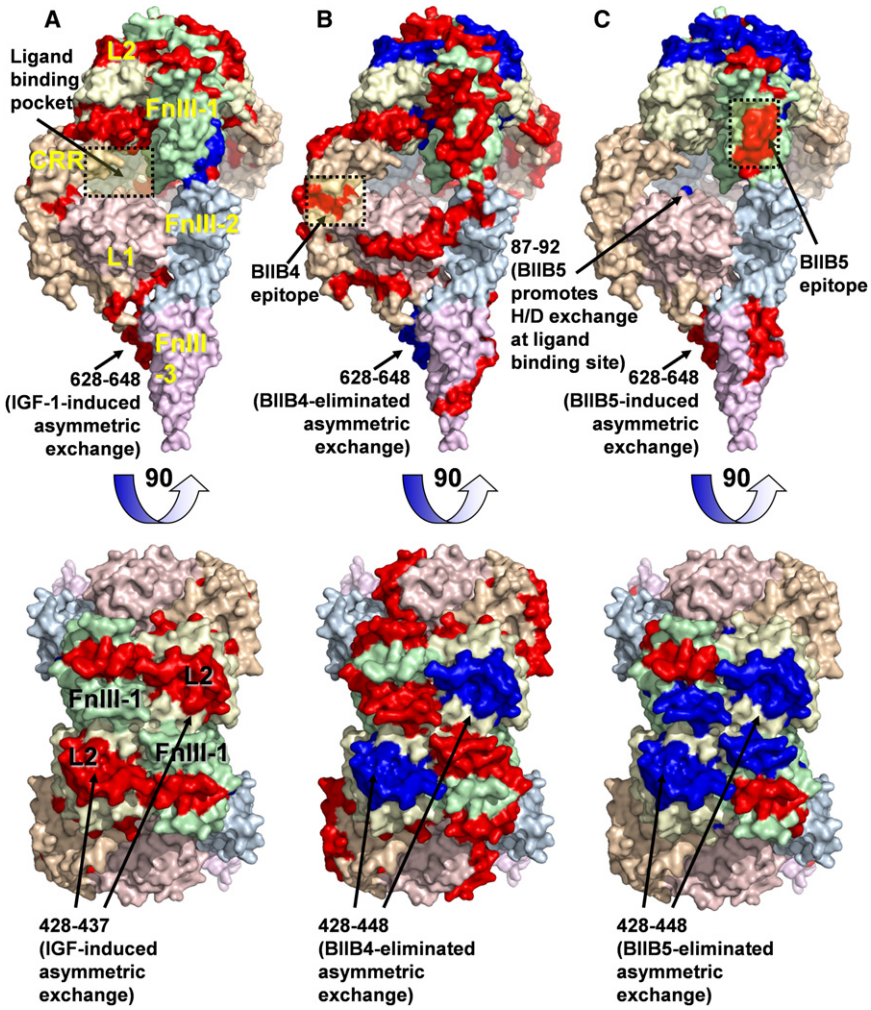

Figure 4. Ligand- and Antibody-Induced Changes in the H/D-Exchange Behavior of hIGF-1R(1–903)

Changes in H/D-exchange in absence and presence of IGF-1 (A), BIIB4 (B), BIIB5 (C) were mapped to the surface of the crystal structure of the insulin receptor (PDB code 2DTG) (McKern et al., 2006). Red indicates protection from exchange (less exchange), and blue indicates increased exchange on the binding of IGF-1, BIIB4 Fab, or BIIB5 Fab. The bottom IR structure orientation shows the IGF-1-, BIIB4-, and BIIB5-induced changes in H/D-exchange in the interface region of IGF-1R/IR (L2 and FnIII-1). The figure is annotated to highlight the ligand-binding pocket (A), the epitopes of BIIB4 (B), and BIIB5 (C), and the two regions of IGF-1R that demonstrated asymmetric H/D exchange.

H/D-exchange patterns at the homodimeric interface, suggesting that ligand binding modifies the arrangement of the two subunits of the receptor homodimer.

The inhibitory antibodies, BIIB4 and BIIB5, both led to significant changes in H/D-exchange patterns across the entire hIGF-1R extracellular region. BIIB5 is known to be an allosteric inhibitor (Doern et al., 2009); however, exactly how it modifies the affinity of the IGFs for IGF-1R was unclear. BIIB5 has previously been shown to reduce the rate of IGF-1 binding to IGF-1R (Doern et al., 2009). Based on the H/D-exchange data, it seems possible that BIIB5 lowers the ligand affinity for the receptor by disorganizing the ligand-binding site and forcing the ligand to provide an additional "organizing step" in the process of its binding. This hypothesis agrees with the reduced rate of binding between the receptor and its ligands in the presence of BIIB5. BIIB4 had a more profound effect on the H/D-exchange patterns of IGF-1R. Binding of BIIB4 clearly led to a strong protective effect on the CRR and flanking L1 and L2 domains—apparently locking the structure down. This correlates well with its known epitope. It also correlates with circular dichroism (CD) data demonstrating a big increase in β sheet propensity on BIIB4 binding, as well as calorimetry data indicating that BIIB4 has a heat capacity of binding (C_P = −1000 cal mol^{-1} $°C^{-1}$) that is much higher than would be expected based on a typical antibody-binding surface (Doern et al., 2009; Geierhaas et al., 2007). Thus, BIIB4 appears to induce strong local and long-range structural changes across the receptor. BIIB4 binding to IGF-1R leads to very distinct changes in the H/D-exchange behavior of the receptor compared with the changes observed with BIIB5. Perhaps this is one reason why the combination of the inhibitory antibodies has such a profound inhibitory affect on the receptor (Dong et al., 2010, 2011). The concerted changes the inhibitors make in the receptor move it further from the activated state induced by IGF-1. CD spectra of a ternary complex of the BIIB4 and BIIB5 Fabs and hIGF-1R(1–903) appear to contain the combination of hIGF-1R(1–903) structural changes induced by each antibody in isolation (Dong et al., 2010). This antibody combination was significantly more effective at reducing IGF-1R signaling and IGF-1R-induced tumor growth in both in vitro and in vivo settings (Dong et al., 2010). Recently, a bispecific antibody has been reported that contains both the BIIB4 and BIIB5 reactivities with the goal of having improved efficacy in clinical trials over monospecific anti-IGF-1R antibodies that are currently under clinical evaluation (Doern et al., 2009; Pollak, 2008).

Perhaps the most interesting discovery with regards to the H/D-exchange behavior of IGF-1R was the existence of two asymmetrically exchanging populations within the receptor. Asymmetry is known to be an important facet of the signaling of both the IR and epidermal-like growth factor receptor (EGFR) families. Only recently have many of the structural features behind the asymmetric signaling within the EGFR family been elucidated (Alvarado et al., 2010; Zhang et al., 2006). While asymmetry has been associated with IR/IGF-1R ligand binding for nearly forty years (Christoffersen et al., 1994;

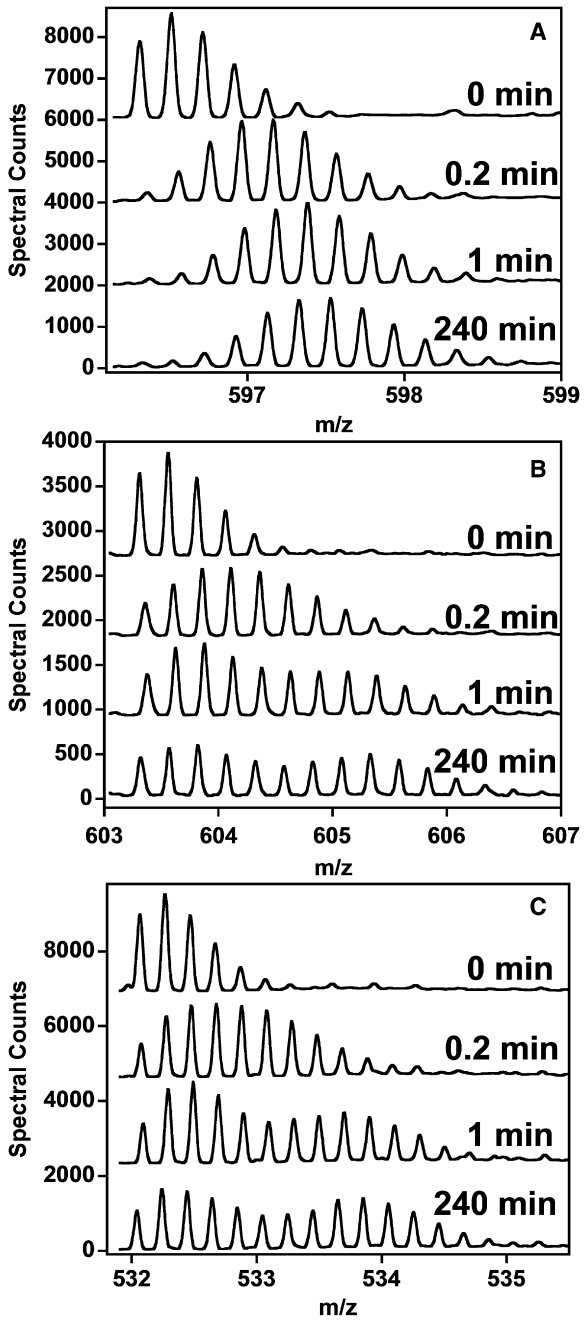

Figure 5. Mass Envelopes at Increasing Time Points for Peptides Demonstrating Both Typical and Asymmetric H/D Exchange

Shown are the peptide mass envelopes (top to bottom) of peptides 466–489 (A), 428–448 (B), and 628–648 (C). Peptide 466–489 (A) is a highly representative H/D-exchange profile showing an overall shift in the mass envelope upon H/D incorporation. Peptides 428–448 (B) and 628–648 (C) were found to have asymmetric H/D-exchange patterns, where two populations of each peptide appear to exchange at different rates—suggesting that each peptide exists in two separate chemical environments. The shifting of the centroid of both isotopic populations indicates this phenomenon is not EX1-exchange behavior.

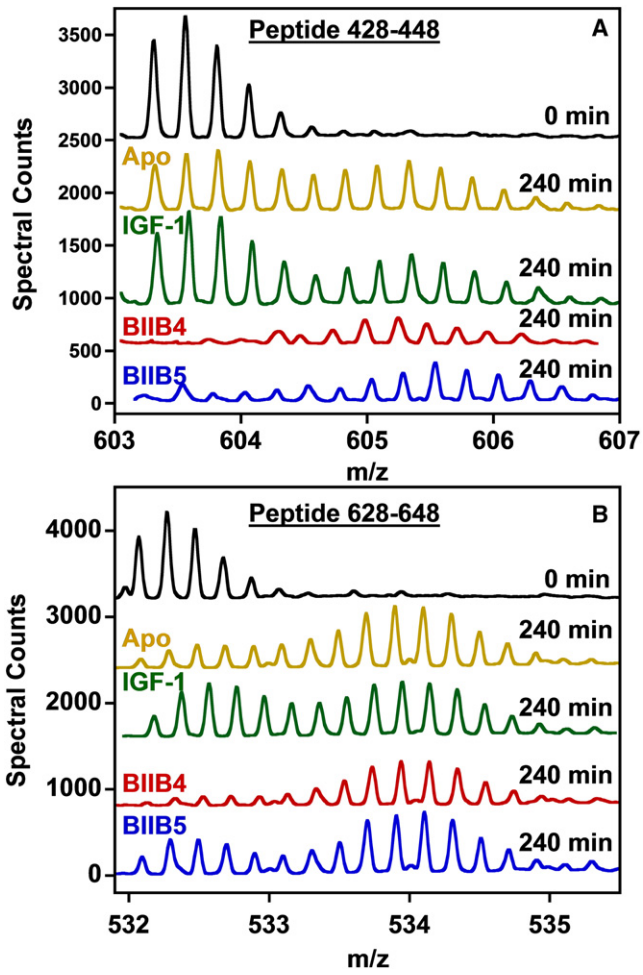

Figure 6. Ligand- and Antibody-Induced Changes in the Asymmetric H/D-Exchange Populations of Peptides 428–448 and 628–648

Shown are the mass envelopes of peptides 428–448 (A) and 628–648 (B) of hIGF-1R(1–903) after 240 min of H/D exchange in the absence and presence of IGF-1 or the inhibitory antibodies.

De Meyts et al., 1973), little regarding defined structural aspects of the asymmetric state of the receptors has been elucidated—even though global conformational studies have been described recently (Whitten et al., 2009). We found two regions of hIGF-1R (residues 428–448 in L2 near the homodimeric interface and residues 628–648 adjacent to the ID) that demonstrated two distinct H/D-exchange populations in apo-hIGF-1R(1–903) (Figures 5A and 5B). There is no formal way of ruling out that this asymmetry is associated with two separate conformations of the receptor in two separate molecules (i.e., not within the same homodimer). However, because IGF-1R displays strong negative cooperativity when binding ligand (Christoffersen et al., 1994; De Meyts et al., 1973) and the protected population of both peptides is always fractional in the presence of ligand (Figures 6A and 6B), it seems likely the two states represent an asymmetric environment within each homodimeric molecule that is favored on ligand binding. Asymmetry within each of the homodimeric subunits (i.e., each L1-CRR-L2-FnIII-1-FnIII-2-FnIII-3 half of the receptor) might be expected if each subunit were to adopt distinct

conformations. Residues 428–448 are near the homodimeric interface, and residues 628–648 are adjacent to residues 669–672 that are involved in interdimer disulfide-bond formation (Adams et al., 2000). The adoption of distinct conformations within each homodimeric subunit near these interfacial regions may play a role in both of these peptides inhabiting two distinct chemical environments.

In the 628–648 peptide in particular, the population that exchanged more slowly, dubbed the protected state, was present in apo-IGF-1R at a much lower population than the more rapidly exchanging state. If the asymmetric state represents the active conformation of the receptor, then this protected state population may reflect a low level of constitutive activity, even in the absence of ligand. Indeed, we have observed that the full-length receptor demonstrates a low level of autophosphorylation even in the apo-state (S.J.D., E. Langley, and J. Dong, unpublished data). This may be another indication that the population of the protected state of the 628–648 peptide provides a measure of the active population of IGF-1R. Why the population of the protected state within residues 428–448 (in apo-IGF-1R) differed from what was observed for residues 628–648 remains a mystery.

All three activity modifying agents (IGF-1, BIIB4, and BIIB5) induced significant changes in the H/D-exchange behavior of the two peptides, 428–448 and 628–648, which exist in two distinct chemical environments, away from the H/D-exchange observed within apo-hIGF-1R. Saturation of the receptor with IGF-1 led to a significant increase in the population of the protected state of each of these peptides. The competitive inhibitor, BIIB4, entirely eliminated the protected states of both peptides, potentially forcing the receptor into a completely symmetrical and inactive state. The allosteric inhibitor, BIIB5, led to a complex modification of these asymmetric peptides, eliminating the protected state within residues 428–448, while enhancing the protected state within residues 628–648. Surinya et al. (2002) describe the inhibitory activities of an anti-IR antibody (47–9) with a similar epitope as BIIB5. Like insulin, the 47-9 antibody could accelerate ^{125}I-insulin dissociation from the receptor—a hallmark of negative cooperativity. The antibody could only induce accelerated ^{125}I-insuiln release if residues 650–704 (636–690 of IGF-1R) were included in the soluble IR extracellular domain construct. This region overlaps with residues 641–648 where we demonstrate the asymmetry to originate from and whose population of the protected state is enhanced by both IGF-1 and BIIB5 (even though BIIB5 can clearly occupy both its receptor epitopes simultaneously (Doern et al., 2009) and eliminates the protected state of residues 428–448). Thus, there is some precedence for residues 636–690 being involved in negative cooperativity. Although the data with the allosteric inhibitor is ambiguous in terms of its effect on receptor symmetry, it is clear that ligand binding enhances receptor asymmetry whereas the competitive inhibitor appears to trap the receptor in a symmetric environment. The populations of the "protected states" of these two peptides thus appear to serve as nonposttranslational modification reporters of the active/inactive states of IGF-1R. The ability to quantify the asymmetry may be useful for the design of biologic therapeutics targeting the receptor or ultimately as markers in a translational medicine setting that quantify IGF-1R activity in tumor patients and whether they respond to anti-IGF-1R therapy.

EXPERIMENTAL PROCEDURES

hIGF-1R(1–903), IGF-1, BIIB4 Fab, and BIIB5 Fab

The hIGF-1R(1–903) protein with a C-terminal 10 histidine tag was produced in chinese hamster ovary (CHO) cells and purified as described previously (Doern et al., 2009). Human IGF-1 was from R&D Systems. BIIB4 and BIIB5 Fabs were produced as described previously (Doern et al., 2009).

Deglycosylation of hIGF-1R(1–903)

The hIGF-1R(1–903) protein (4 mg at 1.5 mg/ml) was dialyzed into 20 mM Tris, pH 8.0. The N-glycanase PNGaseF (Prozyme) was added (2 units), and the mixture was incubated overnight at room temperature. The deglycosylated protein was purified from PNGaseF and detached glycan using a preparative Superdex200 SEC column linked to an AKTA Explorer (GE Healthcare). The SEC column was pre-equilibrated in phosphate buffered saline (PBS).

Characterization of Deglycosylated hIGF-1R(1–903)

Deglycosylated hIGF-1R(1–903) protein was compared with untreated hIGF-1R(1–903) by SDS-PAGE, differential scanning calorimetry (DSC), analytical SEC with in-line static light scattering, and surface plasmon resonance (SPR). For SDS-PAGE analysis, 5 μg nonreduced and 10 μg reduced samples (heated in 200 mM DTT) were applied to 4%–12% NuPAGE Bis-Tris gels using the buffers and protocols of the manufacturer (Life Technologies).

DSC scans were performed using an automated capillary DSC (capDSC, GE Healthcare). PNGase treated and untreated hIGF-1R(1–903) protein solutions and reference (buffer) solutions were sampled automatically from a 96-well plate using the robotic attachment. Before each protein scan, two buffer scans were performed to define the baseline for subtraction. All 96-well plates containing protein were stored within the instrument at 6°C. Each sample was run at 0.5 mg/ml in PBS. Scans were performed from 10°C–95°C at 2°C/min using the low feedback mode. Scans were analyzed using the Origin software supplied by the manufacturer. Subsequent to the subtraction of reference baseline scans, nonzero protein scan baselines were corrected using a third-order polynomial.

For quantitative molecular size determination, 30 μg of deglycosylated and untreated hIGF-1R(1–903) were individually injected onto a Phenomenex BioSep-SEC-s3000 7.8 mm × 30 cm analytical SEC column equilibrated in 10 mM phosphate, 150 mM NaCl, 0.02% NaN_3 at pH 6.8 using an Agilent 1100 HPLC system. Light scattering data for material eluting from the SEC column were collected using a miniDAWN static light scattering detector coupled to an in-line refractive index meter (Wyatt Technologies). Ultraviolet data were analyzed using HPCHEM (Agilent), and light scattering data were analyzed using ASTRA V (Wyatt).

All SPR experiments were performed on a Biacore 3000 set to 25°C using HBS-EP running buffer (GE Healthcare). An anti-HisTag antibody (PENTA-His, QIAGEN) was immobilized to 10,000 resonance units (RUs) on a CM5 chip surface at 20 μg/ml in 10 mM acetate, pH 4.0 using the standard amine chemistry protocols provided by the manufacturer. hIGF-1R(1–903) (untreated or treated with PNGaseF) was captured on the PENTA-His surface by injecting 20 μl of 40 nM protein at 2 μl/min. On capture of either treated or untreated hIGF-1R(1–903), 160 μl injections of 30 nM and 3 nM solutions of BIIB4 or BIIB5 Fabs were injected at 20 μl/min followed by a 30 min dissociation period with a constant flow of HBS-EP buffer. Alternately, 50 nM and 5 nM solutions of IGF-1 were injected in place of the Fabs. Each injection series was regenerated using 2 × 10 μl injections of 0.1 M glycine, pH 2.0, at 60 μl/min. Each curve was double referenced using (1) data obtained from a blocked surface devoid of the PENTA-His antibody; and (2) data from a primary injection of hIGF-1R(1–903), followed by a secondary injection of HBS-EP buffer.

H/D-Exchange Mass Spectrometry

H/D-exchange was performed as previously described (Houde et al., 2009). The time course for labeling was 10 s, 1 min, 10 min, 60 min, and 240 min. Deuterium labeling was quenched by reducing the pH to 2.5–2.6 and lowering the temperature to 0°C. Quenched samples were digested online with pepsin, desalted, and separated using a special Waters UPLC system designed for H/D-exchange (Wales et al., 2008). A 9-min linear acetonitrile gradient (2%–40%) was used to separate the peptides; both mobile phases contained 0.05% formic acid. Eluate from the C18 column was directed into a Waters

QTof Synapt HD mass spectrometer with electrospray ionization and lock-mass correction (using Glu-fibrinogen peptide). Mass spectra were acquired from m/z 255 to 1800. Pepsin fragments were identified using replicate injections and a combination of exact mass and MS^E, aided by Waters Identity^E software (Silva et al., 2006). Peptide deuterium levels were determined using the Excel-based program HX-Express (Weis et al., 2006a) and other custom macros. No adjustment was made for deuterium back-exchange during the analysis; therefore, all results are reported as relative deuterium level (Wales and Engen, 2006). Approximately 94% of the hIGF-1R amino acid sequence was covered by the peptic fragments in these experiments, which constituted over 200 identified peptides (Table S1). Each analysis was repeated two to four times over the course of several months, and each protein injection was followed with column washing and two buffer blank injections. Based on our observations using repeat injections, we found that the error associated with deuterium level determination was 0.1–0.3 Da (that is, ±0.05–0.15 Da for each data point), similar to that reported elsewhere (Burkitt and O'Connor, 2008).

Determination of Saturating Ligand/Fab Conditions for H/D-Exchange Mass Spectrometry Binding Experiments

Conditions were derived where hIGF-1R(1–903) would be ≥98% in the IGF-1-, BIIB4 Fab-, or BIIB5 Fab-bound state (Engen, 1999; Sancho et al., 1991). For two interacting proteins, the equilibrium dissociation constant, K_D, is described as

$$P + L \Leftrightarrow PL; K_D = \frac{P_F L_F}{PL_B}; P_F = P_T - PL_B; L_F = L_T - PL_B, \quad (1)$$

where P is hIGF-1R(1–903), L is IGF-1, BIIB4, or BIIB5, PL is the complex between hIGF-1R(1–903) and any of the ligands, P_F and L_F are the concentrations of hIGF-1R(1–903) and ligand, respectively, unbound in solution, P_T and L_T are the total concentrations of each component in solution, and PL_B is the concentration of the binary complex of ligand and receptor. Substituting for P_F and L_F leads to the following:

$$\frac{(P_T - PL_B)(L_T - PL_B)}{PL_B} = K_D. \quad (2)$$

Equation 2 can be rearranged into a quadratic equation to solve for PL_B:

$$PL_B = \frac{(K_D + P_T + L_T) \pm \sqrt{(K_D + P_T + L_T)^2 + 4(P_T)(L_T)}}{2}. \quad (3)$$

P_F and L_F can then be determined from Equation 1 enabling the percentages of free versus bound protein to be estimated. The affinities of IGF-1, BIIB4, and BIIB5 for hIGF-1R(1–903) have been determined to be 20 nM, 4 nM, and 1.5 nM, respectively (Doern et al., 2009). To analyze the H/D-exchange behavior of hIGF-1R(1–903) in the IGF1-bound state, the labeling solution consisted of 250 nM hIGF-1R(1–903) (based on its monomeric molecular weight of 105 kDa) and 1.6 μM IGF-1. Under these conditions, the receptor was expected to be 98.5% in the IGF-1-bound state at equilibrium. To analyze the H/D-exchange behavior of hIGF-1R(1–903) in the presence of the antibody inhibitors, the labeling solutions consisted of 300 nM hIGF-1R(1–903) and 460 nM BIIB4 Fab or 600 nM BIIB5 Fab where the receptor was expected to be 97.7% and 98.5% in the Fab-bound states, respectively.

SUPPLEMENTAL INFORMATION

Supplemental Information includes one table and can be found with this article online at doi:10.1016/j.str.2011.03.014.

ACKNOWLEDGMENTS

The authors acknowledge Drs. Steven Berkowitz and Helena Madden for supporting the project, Dr. John R. Engen for helpful discussions, and Dr. Kristin Demarest for editing the manuscript.

Received: January 11, 2011
Revised: March 1, 2011
Accepted: March 13, 2011
Published: June 7, 2011

REFERENCES

Adams, T.E., Epa, V.C., Garrett, T.P.J., and Ward, C.W. (2000). Structure and function of the type 1 insulin-like growth factor receptor. Cell. Mol. Life Sci. *57*, 1050–1093.

Alvarado, D., Klein, D.E., and Lemmon, M.A. (2010). Structural basis for negative cooperativity in growth factor binding to an EGF receptor. Cell *142*, 568–579.

Burkitt, W., and O'Connor, G. (2008). Assessment of the repeatability and reproducibility of hydrogen/deuterium exchange mass spectrometry measurements. Rapid Commun. Mass Spectrom. *22*, 3893–3901.

Christoffersen, C.T., Bornfeldt, K.E., Rotella, C.M., Gonzales, N., Vissing, H., Shymko, R.M., ten Hoeve, J., Groffen, J., Heisterkamp, N., and De Meyts, P. (1994). Negative cooperativity in the insulin-like growth factor-I receptor and a chimeric IGF-1/insulin receptor. Endocrinology *135*, 472–475.

Clemmons, D.R. (2007). Modifying IGF1 activity: an approach to treat endocrine disorders, atherosclerosis, and cancer. Nat. Rev. Drug Discov. *6*, 821–833.

De Meyts, P., and Whittaker, J. (2002). Structural biology of insulin and IGF1 receptors: implications for drug design. Nat. Rev. Drug Discov. *1*, 769–783.

De Meyts, P., Roth, J., Neville, D.M., Gavin, J.R., and Lesniak, M.A. (1973). Insulin interactions with its receptors: experimental evidence for negative cooperativity. Biochem. Biophys. Res. Commun. *55*, 154–161.

Doern, A., Cao, X., Sereno, A., Reyes, C.L., Alshuler, A., Huang, F., Hession, C., Flavier, A., Favis, M., Tran, H., et al. (2009). Characterization of inhibitory anti-insulin-like growth factor receptor antibodies with different epitope specificity and ligand-blocking properties. J. Biol. Chem. *284*, 10254–10267.

Dong, J., Demarest, S.J., Sereno, A., Tamraz, S., Langley, E., Doern, A., Snipas, T., Perron, K., Joseph, I., Glaser, S.M., et al. (2010). Combination of two insulin-like growth factor-I receptor inhibitory antibodies targeting distinct epitopes leads to an enhanced antitumor response. Mol. Cancer Ther. *9*, 2593–2604.

Dong, J., Sereno, A., Snyder, W.B., Miller, B.R., Tamraz, S., Doern, A., Favis, M., Wu, X., Tran, H., Langley, E., et al. (2011). Stable IgG-like bispecific antibodies directed towards the type I insulin-like growth factor receptor demonstrate enhanced ligand blockade and anti-tumor activity. J. Biol. Chem. *286*, 4703–4717.

Engen, J.R. (1999). Analysis of Unfolding and Protein Dynamics in the Regulatory Domains of Hematopoietic Cell Kinase with Hydrogen Deuterium Exchange and Mass Spectrometry (Lincoln: University of Nebraska).

Englander, S.W., and Kallenbach, N.R. (1983). Hydrogen exchange and structural dynamics of proteins and nucleic acids. Q. Rev. Biophys. *16*, 521–655.

Fang, J., Rand, K.D., Beuning, P.J., and Engen, J.R. (2011). False EX1 signatures caused by sample carryover during HX MS analyses. Int. J. Mass Spectrom. *302*, 19–25.

Garrett, T.P.J., McKern, N.M., Lou, M., Frenkel, M.J., Bentley, J.D., Lovrecz, G.O., Elleman, T.C., Cosgrove, L.J., and Ward, C.W. (1998). Crystal structure of the first three domains of the type-1 insulin like growth factor receptor. Nature *394*, 395–399.

Gavin, J.R., Gorden, P., Roth, J., Archer, J.A., and Buell, D.N. (1973). Characteristics of the human lymphocyte insulin receptor. J. Biol. Chem. *248*, 2202–2207.

Geierhaas, C.D., Nickson, A.A., Lindorff-Larsen, K., Clarke, J., and Vendruscolo, M. (2007). BPPred: a web-based computational tool for predicting biophysical parameters of proteins. Protein Sci. *16*, 125–134.

Houde, D., Arndt, J., Domeier, W., Berkowitz, S., and Engen, J.R. (2009). Characterization of IgG1 conformation and conformational dynamics by hydrogen/deuterium exchange mass spectrometry. Anal. Chem. *81*, 2644–2651.

McKern, N.M., Lawrence, M.C., Streltsov, V.A., Lou, M.Z., Adams, T.E., Lovrecz, G.O., Elleman, T.C., Richards, K.M., Bentley, J.D., Pilling, P.A., et al. (2006). Structure of the insulin receptor ectodomain reveals a folded-over conformation. Nature *443*, 218–221.

Pollak, M. (2008). Insulin and insulin-like growth factor signalling in neoplasia. Nat. Rev. Cancer *8*, 915–928.

Rodon, J., DeSantos, V., Ferry, R.J., and Kurzrock, R. (2008). Early drug development of inhibitors of the insulin-like growth factor-I receptor pathway: lessons from the first clinical trials. Mol. Cancer Ther. *7*, 2575–2588.

Sancho, J., Meiering, E.M., and Fersht, A.R. (1991). Mapping transition states of protein unfolding by protein engineering of ligand-binding sites. J. Mol. Biol. *221*, 1007–1014.

Silva, J.C., Gorenstein, M.V., Li, G.Z., Vissers, J.P., and Geromanos, S.J. (2006). Absolute quantification of proteins by LCMSE: a virtue of parallel MS acquisition. Mol. Cell. Proteomics *5*, 144–156.

Smith, D.L., Deng, Y., and Zhang, Z. (1997). Probing the non-covalent structure of proteins by amide hydrogen exchange and mass spectrometry. J. Mass Spectrom. *32*, 135–146.

Smith, B.J., Huang, K., Kong, G., Chan, S.J., Nakagawa, S., Menting, J.G., Shi-Quan, H., Whittaker, J., Steiner, D.F., Katsoyannis, P.G., et al. (2010). Structural resolution of a tandem hormone-binding element in the insulin receptor and its implications for design of peptide agonists. Proc. Natl. Acad. Sci. USA *107*, 6771–6776.

Soos, M.A., Siddle, K., Baron, M.D., Heward, J.M., Luzio, J.P., Bellatin, J., and Lennox, E.S. (1986). Monoclonal antibodies reacting with multiple epitopes on the human insulin receptor. Biochem. J. *235*, 199–208.

Soos, M.A., Field, C.E., Lammers, R., Ullrich, A., Zhang, B., Roth, R.A., Andersen, A.S., Kjeldsen, T., and Siddle, K. (1992). A panel of monoclonal antibodies for the type I insulin-like growth factor receptor. J. Biol. Chem. *267*, 12955–12963.

Surinya, K.H., Molina, L., Soos, M.A., Brandt, J., Kristensen, C., and Siddle, K. (2002). Role of insulin receptor dimerization domains in ligand binding, cooperativity, and modulation by anti-receptor antibodies. J. Biol. Chem. *277*, 16718–16725.

Wales, T.E., and Engen, J.R. (2006). Hydrogen exchange mass spectrometry for the analysis of protein dynamics. Mass Spectrom. Rev. *25*, 158–170.

Wales, T.E., Fadgen, K.E., Gerhardt, G.C., and Engen, J.R. (2008). High-speed and high-resolution UPLC separation at zero degrees Celsius. Anal. Chem. *80*, 6815–6820.

Ward, C.W., Lawrence, M.C., Streltsov, V.A., Adams, T.E., and McKern, N.M. (2008). The insulin and EGF receptor structures: new insights into ligand-induced receptor activation. Trends Biochem. Sci. *32*, 129–137.

Weis, D.D., Engen, J.R., and Kass, I.J. (2006a). Semi-automated data processing of hydrogen exchange mass spectra using HX-Express. J. Am. Soc. Mass Spectrom. *17*, 1700–1703.

Weis, D.D., Wales, T.E., and Engen, J.R. (2006b). Identification of characterization of EX1 kinetics in H/D exchange mass spectrometry by peak width analysis. J. Am. Soc. Mass Spectrom. *17*, 1498–1509.

Whittaker, J., Groth, A.V., Mynarcik, D.C., Pluzek, L., Gadsbøll, V.L., and Whittaker, L.J. (2001). Alanine scanning mutagenesis of a type-1 insulin-like growth factor receptor ligand binding site. J. Biol. Chem. *276*, 43980–43986.

Whitten, A.E., Smith, B.J., Menting, J.G., Margetts, M.B., McKern, N.M., Lovrecz, G.O., Adams, T.E., Richards, K., Bentley, J.D., Trewhella, J., et al. (2009). Solution structure of ectodomains of the insulin receptor family: the ectodomain of the type-1 insulin-like growth factor receptor displays asymmetry of ligand binding accompanied by limited conformational change. J. Mol. Biol. *394*, 878–892.

Zhang, X., Gureasko, J., Shen, K., Cole, P.A., and Kuriyan, J. (2006). An allosteric mechanism for activation of the kinase domain of epidermal growth factor receptor. Cell *125*, 1137–1149.

